

An Online Data-Driven Method to Locate Forced Oscillation Sources from Power Plants Based on Sparse Identification of Nonlinear Dynamics (SINDy)

Yaojie Cai, Xiaozhe Wang, *Senior Member, IEEE*, Geza Joos, *Life Fellow, IEEE*, and Innocent Kamwa, *Fellow, IEEE*

Abstract—Forced oscillations may jeopardize the secure operation of power systems. To mitigate forced oscillations, locating the sources is critical. In this paper, leveraging on Sparse Identification of Nonlinear Dynamics (SINDy), an online purely data-driven method to locate the forced oscillation is developed. Validations in all simulated cases (in the WECC 179-bus system) and actual oscillation events (in ISO New England system) in the IEEE Task Force test cases library are carried out, which demonstrate that the proposed algorithm, requiring no model information, can accurately locate sources in most cases, even under resonance condition and when the natural modes are poorly damped. The little tuning requirement and low computational cost make the proposed method viable for online application.

Index Terms—forced oscillations, low frequency oscillations, resonant systems, Sparse Identification of Nonlinear Dynamics (SINDy)

I. INTRODUCTION

SUSTAINED oscillation is one of the major threats to the security and stability of electric power systems, which may introduce undesirable vibrations, damage power grid equipment, and interrupt power supply. In the most severe scenario, growing oscillations may lead to catastrophic cascading blackouts [1].

Sustained oscillations can be classified into natural oscillations and forced oscillations. Natural (modal) oscillations may result from high-gain fast exciters, malfunction of control devices, weakly tied transmission lines, and load fluctuations [2], while forced oscillations may appear when power systems are excited by external periodic disturbances due to large cyclic loads, erroneous control loops in power plants, etc. [3]. Unlike natural oscillations that have been extensively studied in many previous works (e.g., [4]–[6]), forced oscillations have gained increasing attention recently. IEEE PES Task Force on Oscillation Source Location was established in 2016 as many “new” oscillatory behaviors captured in power grids that could not be reproduced through traditional natural oscillation analysis. Note that the oscillatory behaviors themselves may not be new but were captured recently owing to an increasing coverage of Phasor Measurement Units (PMUs). Further investigations

suggested that they were forced oscillations introduced by specific generators, either under special conditions or with failed components [7]. These observations clearly show that mitigating forced oscillations are significant, imperative yet challenging to ensure the secure operation of power systems. The most effective means to mitigate forced oscillation is to locate and remove/correct the sources.

With the help of synchrophasor technology that provides accurate synchronized measurements with high sampling frequencies, many forced oscillation locating methods have been developed using PMU data. Transfer function based methods have been proposed in [8], which identify sources of forced oscillations from indexes derived from the assumed system transfer function. Effective impedance based methods were developed in [9] to locate forced oscillation sources by comparing the measured current spectrum of system components with predicted ones. However, all the aforementioned works require accurate information of power network and generator model parameters, which may not always be available in practice due to communication errors, bad data, frequent line switching, etc. To relax the assumption of accurate knowledge of power network and dynamic model, purely data-driven methods for forced oscillation locating have been recently developed in [10], [11]. The concept of oscillation phasor estimated from PMU data is utilized in [10] to locate the forced oscillation source, yet the performance of the method under resonance or under low forcing strength is in question as the estimation of oscillation phasor and damping ratio may be deteriorated. The authors of [11] applied Robust Principal Component Analysis (RPCA) to extract the sparse and low-rank components of the measurement matrix, which are linked to the resonance-free and resonance components of system dynamics, while the resonance-free component is used to locate forced oscillations. Despite being intuitive, the theoretical proof of the mapping between the physic model and the low-rank/sparse components remains to be seen. The authors of [12] proposed the Transient Energy Flow (TEF) method that identifies the oscillation source as the one that generates oscillation energy, which has been well tested in [13] with great success. However, as discussed in [11], the TEF method may fail if the source generator is not monitored and erroneous system topology is used.

In this paper, we propose a purely data-driven method to

This work was supported by the Fonds de Recherche du Quebec-Nature et technologies under Grant FRQ-NT PR-298827. (Corresponding author: Xiaozhe Wang.)

locate forced oscillation sources. Leveraging on the methodology of Sparse Identification of Nonlinear Dynamics (SINDy) [14]–[17] that combines compressed sensing technique with nonlinear dynamical systems, we show that the power system dynamic model can be extracted from PMU measurements. As the extracted dynamic equations have a clear physical interpretation, the location of forced oscillation sources can be carried out using the extracted model. The performance of the proposed method has been tested in all 24 cases available in the IEEE Task Force test cases library [18], [19] (18 simulated cases in the WECC 179 bus system and 6 actual oscillation events in ISO New England (ISO-NE) system) using raw PMU data. In sum, the contributions of this paper are presented as below:

- 1) The proposed method is purely data-driven, requiring no information of the dynamic model and the network parameters.
- 2) The proposed method, requiring a little tuning of parameters, and trivial computational cost, possesses good feasibility in practical online applications.
- 3) The proposed method can accurately locate forced oscillation sources in most of the cases available in the library including resonance cases, low forcing strength cases, rectangular forcing signal cases, etc.
- 4) Compared to the RPCA method in [11], the proposed method seems to be more accurate in the cases where the forced signals come from turbine governors of generators, serving as a good complement to the RPCA method. Compared to the Dissipating Energy Flow method in [13], the proposed method may help pinpoint the generators closest to the source generator when the source generators are not monitored, providing useful guidance for source searching.

In addition, the potential reasons for the failure of the method in two cases are discussed. The test results imply that the performance of the proposed method in cases where the forced oscillations are completely unobservable from measurements due to, for example, extremely low forcing strength may deteriorate. Besides, since the library considers only the cases where the source of forced oscillations are from generators (i.e., exciters, turbine governors), future efforts are needed to extend and test the proposed method when the forced oscillation sources are not generators (e.g., HVDC control).

II. POWER SYSTEM DYNAMIC MODEL FOR FORCED OSCILLATION ANALYSIS

The power system dynamics can be described as a set of nonlinear Differential Algebraic Equations (DAE). Particularly, power generator rotor dynamics play critical roles in ambient conditions [20]–[22], which can be represented by the classical swing equations:

$$\begin{aligned} \dot{\boldsymbol{\delta}} &= \boldsymbol{\omega} \\ M\dot{\boldsymbol{\omega}} &= \mathbf{P}_m - \mathbf{P}_e - D\boldsymbol{\omega} + \mathbf{u} \end{aligned} \quad (1)$$

where $\boldsymbol{\delta} = [\delta_1, \dots, \delta_r]^T$; $\boldsymbol{\omega} = [\omega_1, \dots, \omega_r]^T$ are the vectors of rotor angles and angular frequencies of all generators; $M = \text{diag}[M_1, \dots, M_r]$ is a diagonal matrix containing the

inertia constants of all generators; $D = \text{diag}[D_1, \dots, D_r]$ contains the damping coefficients of all generators; $\mathbf{P}_m = [P_{m_1}, \dots, P_{m_r}]^T$ and $\mathbf{P}_e = [P_{e_1}, \dots, P_{e_r}]^T$ denote the vectors of mechanical power and electrical power of generators; \mathbf{u} denotes the external input. In forced oscillation study, \mathbf{u} may represent the periodic forcing imposed on generator shaft due to, for example, inappropriate parameters in the control loop from turbine governor or exciter. Indeed, as shown in Appendix A, the forced oscillations from either excitation systems or turbine governors may manifest themselves in swing equations given in (1). Due to its periodic nature, $\mathbf{u}(t) = [u_1(t), \dots, u_r(t)]^T$ can be described by Fourier series. For each $u_j(t)$, $j \in \{1, 2, \dots, r\}$, it can be represented as:

$$\begin{aligned} u_j(t) &= \sum_{i=1}^l (a_{ij} \sin(\omega_{F_{ij}} t) + b_{ij} \cos(\omega_{F_{ij}} t)) \\ &= \sum_{i=1}^l \left(\sqrt{a_{ij}^2 + b_{ij}^2} \sin(\omega_{F_{ij}} t + \varphi_{ij}) \right) \\ &= \sum_{i=1}^l \left(\sqrt{\zeta_{ij}} \sin(\omega_{F_{ij}} t + \varphi_{ij}) \right) \end{aligned} \quad (2)$$

where $\zeta_{ij} = a_{ij}^2 + b_{ij}^2$, $\varphi_{ij} = \arctan(\frac{b_{ij}}{a_{ij}})$. Besides, the electrical power injection to the grid from generator i :

$$P_{e_i} = E_i^2 G_{ii} + \sum_{i=1, j \neq i}^r E_i E_j Y_{ij} \cos(\phi_{ij} - \delta_i + \delta_j) \quad (3)$$

where E_i is the i th generator internal electromotive force (emf) magnitude. $Y_{ij} \angle \phi_{ij} = G_{ij} + jB_{ij}$ corresponds to the $(i, j)^{th}$ entry of the reduced admittance matrix. As discussed in [23], power systems are naturally experiencing random perturbations from load power variations, which can be reflected in the diagonal elements of the equivalent admittance matrix Y seen from the generator internal buses:

$$Y(i, i) = Y_{ii} (1 + \sigma_{load_i} \eta_i) \angle \phi_{ii} \quad (4)$$

where σ_{load_i} is the standard deviation of load variation. η_i is a standard Gaussian random variable. It is typically assumed that the random variation does not affect ϕ_{ii} such that load power factor remains constant [23] in a time window of minutes considering the fact that power factor correction is carried out in hourly time scale. Thus, the swing equation considering stochastic load variation can be represented as [21] [24]:

$$\begin{aligned} \dot{\boldsymbol{\delta}} &= \boldsymbol{\omega} \\ M\dot{\boldsymbol{\omega}} &= \mathbf{P}_m - \mathbf{P}_e - D\boldsymbol{\omega} - E^2 G \Sigma \boldsymbol{\eta} + \mathbf{u} \end{aligned} \quad (5)$$

where $E = \text{diag}[E_1, \dots, E_r]$; $G = \text{diag}[G_{11}, \dots, G_{rr}]$; $\Sigma = \text{diag}[\sigma_{load_1}, \dots, \sigma_{load_r}]$; $\boldsymbol{\eta} = [\eta_1, \dots, \eta_r]^T$; Similar to [9], [25], the classical generator model is considered in this study as we are interested in system dynamics in ambient conditions. Nevertheless, the performance of the proposed method is tested when higher-order generator models with detailed control devices are implemented, as well as in the actual oscillation events with no information about the dynamical model, as shown in Section V-VI. Besides, the performance of the method is also tested under load power factor variations as presented in Section V-E. These results further confirm that the rotor dynamics described in (5) are sufficient for locating forced oscillation sources.

Under small perturbation, (5) can be linearized around its steady-state operating point as below:

$$\begin{bmatrix} \Delta \dot{\delta} \\ \Delta \dot{\omega} \end{bmatrix} = \begin{bmatrix} 0_{r \times r} & I_{r \times r} \\ -M^{-1} \frac{\partial P_e}{\partial \delta} & -M^{-1} D \end{bmatrix} \begin{bmatrix} \Delta \delta \\ \Delta \omega \end{bmatrix} + \begin{bmatrix} \mathbf{0}_{r \times 1} \\ -M^{-1} E^2 G \Sigma \boldsymbol{\eta} \end{bmatrix} + \begin{bmatrix} \mathbf{0}_{r \times 1} \\ \mathbf{u} \end{bmatrix} \quad (6)$$

As can be seen that the governing dynamic equations consist of linear terms, noise terms, and forced oscillation terms, i.e., the three terms on the right-hand side of (6), respectively.

In this paper, we will exploit the structure of power system physical model to develop a novel method based on SINDy to estimate the terms particularly corresponding to the forced oscillations purely from PMU measurements. The magnitude of the terms can be used to locate the sources of forced oscillations. In the next section, the essence and theoretical basis of SINDy method will be briefly introduced.

III. SPARSE IDENTIFICATION OF NONLINEAR DYNAMICS

Let's consider a generic dynamical system of the following form:

$$\dot{\mathbf{x}} = \mathbf{h}(\mathbf{x}) \quad (7)$$

where \mathbf{x} is the vector of state variables; \mathbf{h} are the governing equations describing the dynamics of the system. The core observation is that for many dynamical systems including power systems, the function \mathbf{h} is sparse in the space of possible functions (more explanation after (12) for power system model). In light of this, a sparse identification method of finding the underlying dynamics SINDy is introduced in [14], which can identify the governing equations from measurement data by leveraging advances in sparsity techniques and machine learning. The exploited sparse formulation nicely balances the model complexity (i.e., the sparsity of governing equations) and accuracy, avoiding overfitting the model to the data.

In particular, given measurement matrix $X^T = [\mathbf{x}(t_1), \dots, \mathbf{x}(t_m)]$ and its time derivative matrix \dot{X} either measured or numerically approximated, \dot{X} can be represented as a linear combination of columns from a feature library Θ :

$$\dot{X} = \Theta(X) \Xi \quad (8)$$

where the feature library

$$\Theta(X) = \begin{bmatrix} \Theta_1(X) & \dots & \Theta_i(X) \\ \vdots & \ddots & \vdots \end{bmatrix} \quad (9)$$

may consist of candidate linear or nonlinear functions such as constants, polynomials, trigonometric functions, etc. $\Xi = [\boldsymbol{\xi}_1, \boldsymbol{\xi}_2, \dots, \boldsymbol{\xi}_v]$ contains the sparse vectors of coefficients to be determined. Once Ξ is determined, the dynamics of each state variable can be represented as (10).

$$\dot{\mathbf{x}}_k = \mathbf{h}_k(\mathbf{x}) = \Theta(\mathbf{x}^T) \boldsymbol{\xi}_k \quad k = \{1, 2, \dots, v\} \quad (10)$$

Note that $\Theta(\mathbf{x}^T)$ is a vector of symbolic functions of \mathbf{x} while $\Theta(X)$ is a matrix. Solving $\boldsymbol{\xi}_k$ requires distinct optimization for each k . More details will be discussed in Section IV. SINDy framework has been further extended to include external inputs and feedback (e.g., [16], [17])

The choice of basis functions Θ is crucial to achieve the sparse dynamics, which nevertheless may not be clear for general dynamical systems and may even require advanced algorithms in machine learning to extract features [14]. However, in the forced oscillation study of power systems, a reasonable choice of nonlinear functions can be selected because of the periodic nature of forced oscillations and the physical model of power system as discussed in Section IV.

In short, SINDy method includes building a library of basis functions for seeking a linear relationship between the basis functions and the time derivatives of measurement data, and a sparse regression method to estimate the coefficient matrix Ξ that balances sparsity and accuracy.

IV. A DATA-DRIVEN METHOD TO LOCATE FORCED OSCILLATIONS

If we substitute $\mathbf{u}(t) = [u_1(t), \dots, u_r(t)]^T$ in (2) to the linearized power system stochastic dynamic model, (5), then the power system model can be represented as:

$$\begin{bmatrix} \Delta \dot{\delta} \\ \Delta \dot{\omega} \end{bmatrix} = \begin{bmatrix} 0_{r \times r} & I_{r \times r} \\ -M^{-1} \frac{\partial P_e}{\partial \delta} & -M^{-1} D \end{bmatrix} \begin{bmatrix} \Delta \delta \\ \Delta \omega \end{bmatrix} + \begin{bmatrix} \mathbf{0}_{r \times 1} \\ -M^{-1} E^2 G \Sigma \boldsymbol{\eta} \end{bmatrix} + \begin{bmatrix} \mathbf{0} \\ \mathbf{a}_1 \end{bmatrix} \sin(\omega_{F_1} t) + \begin{bmatrix} \mathbf{0} \\ \mathbf{b}_1 \end{bmatrix} \cos(\omega_{F_1} t) + \dots + \begin{bmatrix} \mathbf{0} \\ \mathbf{b}_n \end{bmatrix} \cos(\omega_{F_n} t) \quad (11)$$

where $\omega_{F_i}, i \in \{1, 2, \dots, n\}$ are the dominant forced oscillation frequencies. It can also be represented in a compact form:

$$\begin{bmatrix} \Delta \dot{\delta} \\ \Delta \dot{\omega} \end{bmatrix} = \begin{bmatrix} \mathbf{0} & -M^{-1} E^2 G \Sigma \boldsymbol{\eta} \\ 0 & -M^{-1} \frac{\partial P_e}{\partial \delta} \\ I & -M^{-1} D \\ \mathbf{0} & \mathbf{a}_1 \\ \mathbf{0} & \mathbf{b}_1 \\ \vdots & \vdots \\ \mathbf{0} & \mathbf{a}_n \\ \mathbf{0} & \mathbf{b}_n \end{bmatrix}^T \begin{bmatrix} 1 \\ \Delta \delta \\ \Delta \omega \\ \sin(\omega_{F_1} t) \\ \cos(\omega_{F_1} t) \\ \vdots \\ \sin(\omega_{F_n} t) \\ \cos(\omega_{F_n} t) \end{bmatrix} \quad (12)$$

where $\mathbf{a}_i = [a_{i1}, \dots, a_{ir}]$, $\mathbf{b}_i = [b_{i1}, \dots, b_{ir}]$, describing the magnitudes of potential forced oscillation inputs. This formulation indicates that the power system dynamic model \mathbf{h} is sparse in the function space of zero-degree polynomial bias, linear functions and trigonometric functions.

We can further define the measurement matrix X as below, where machine rotor angles can be obtained, for example, from mechanical speed measurement units of synchrophasor. [26],

$$X = \begin{bmatrix} \Delta \delta_1(t_1) & \dots & \Delta \delta_r(t_1) \\ \vdots & \ddots & \vdots \\ \Delta \delta_1(t_m) & \dots & \Delta \delta_r(t_m) \\ \Delta \omega_1(t_1) & \dots & \Delta \omega_r(t_1) \\ \vdots & \ddots & \vdots \\ \Delta \omega_1(t_m) & \dots & \Delta \omega_r(t_m) \end{bmatrix} \quad (13)$$

$$\dot{X} = \begin{bmatrix} \Delta \dot{\delta}_1(t_1) & \dots & \Delta \dot{\omega}_r(t_1) \\ \vdots & \ddots & \vdots \\ \Delta \dot{\delta}_1(t_m) & \dots & \Delta \dot{\omega}_r(t_m) \end{bmatrix} \quad (14)$$

In case the generator rotor angles and speeds are not time-synchronously measured, the measurements of the voltage angles and frequencies from PMU data are good replacements to the rotor signals as discussed in [27]. This is also validated by the results of actual oscillation events presented in Section VI, in which voltage angles at generator terminal buses from PMUs are directly applied. Besides, δ and ω in ambient conditions may also be estimated from PMU measurements [28], or directly measured [29]. Lastly, if $\Delta\dot{\omega}$ is unavailable, a finite difference approximation can be applied to $\Delta\omega$ for estimating $\Delta\dot{\omega}$.

Then using the measurement matrix X and taking transpose for both sides of (12), we can represent the power system model in the form of $\dot{X} = \Theta(X)\Xi$, i.e., the formulation used in SINDy, where the feature library can be selected naturally as:

$$\Theta(X) = \begin{bmatrix} | & | & \cdots & | & | & \cdots \\ \mathbf{1} & \Delta\delta_1 & \cdots & \Delta\delta_r & \Delta\omega_1 & \cdots \\ | & | & \cdots & | & | & \cdots \end{bmatrix} \quad (15)$$

$$\begin{bmatrix} | & \cdots & | & | & \cdots \\ \Delta\omega_r & \cdots & \sin(\omega_{F_i} t) & \cos(\omega_{F_i} t) & \cdots \\ | & \cdots & | & | & \cdots \end{bmatrix}_{m \times (1+2r+2n)}$$

and, in theory, the coefficient Ξ matrix should be as follows:

$$\Xi = \begin{bmatrix} \Xi_\eta & \Xi_{\text{Jacobian}} & \Xi_{ab} \end{bmatrix}_{2r \times (1+2r+2n)} \quad (16)$$

$$\Xi_\eta = \begin{bmatrix} 0 \\ -M^{-1}E^2G\Sigma\eta \end{bmatrix}_{2r \times 1} \quad (17)$$

$$\Xi_{\text{Jacobian}} = \begin{bmatrix} 0 & I \\ -M^{-1}\frac{\partial P_e}{\partial \delta} & -M^{-1}D \end{bmatrix}_{2r \times 2r} \quad (18)$$

$$\Xi_{ab}^T = \begin{bmatrix} 0 & \cdots & a_{11} & \cdots & a_{1r} \\ \vdots & \cdots & b_{11} & \cdots & b_{1r} \\ \vdots & \ddots & \vdots & \ddots & \vdots \\ \vdots & \cdots & a_{n1} & \cdots & a_{nr} \\ 0 & \cdots & b_{n1} & \cdots & b_{nr} \end{bmatrix}_{2n \times 2r} \quad (19)$$

where the coefficients a_{ij} and b_{ij} , $i \in \{1, 2, \dots, n\}$, $j \in \{1, 2, \dots, r\}$ describe the magnitude of the input forced oscillation of ω_{F_i} at the j th generator. When forced oscillations are contained in X , Ξ_{ab} is a sparse matrix with large magnitudes only corresponding to the forced oscillation frequencies at the source generators. Thus, from the estimated Ξ_{ab} , we can identify the sources of forced oscillations. It is worth noting that a_{ij} and b_{ij} , or more specifically $\sqrt{a_{ij}^2 + b_{ij}^2}$, describes the magnitude of the potential input forced oscillation u_j at frequency ω_{F_i} (see (2)) that is different from the oscillation magnitudes observed from the state variables $[\Delta\delta, \Delta\omega]$ or other measurements (e.g., voltage magnitudes). Besides, SINDy intrinsically can handle both linear and nonlinear dynamics (e.g. [16]). Since we consider sustained oscillations in ambient conditions rather than ring-down signals, the linearized power system model (6) can be applied to describe the system dynamics.

From (15), it can be seen that the forced oscillation frequencies need to be estimated first in order to build up the feature library $\Theta(X)$. To this end, Fast Fourier Transform (FFT) is applied to the measurement matrix X in (13). The

z-score based peak detection method [30] is used to capture the candidates for forced oscillation frequencies $\{\omega_{F_i}\}_i$ from the spectrum for each measurement. In brief, z-score is an index that describes the relationship of a measurement to the mean of a group of values. A z-score of 1.0 means that the measurement's standard deviation is 1 away from the group mean. The statistical dispersion gives a good indication for the anomaly such as the peak in the spectrum. Once peak frequencies are identified for all measurements, we collect n final candidate frequencies by $\Omega_F = \bigcap_{i=1}^{2r} \{\omega_{F_i}\}_i$. It should be noted that Ω_F may contain frequencies of both natural oscillations and forced oscillations.

Once the feature library is built, we need to solve Ξ . A sequential thresholded least square fitting sparse regression process developed in [14] is applied in this paper, which starts with an initial estimation Ξ^0 from the least square fit:

$$\Xi^0 = \Theta_X^\dagger \dot{X} \quad (20)$$

where $\Theta_X^\dagger = (\Theta_X^T \Theta_X)^{-1} \Theta_X^T$ denotes the pseudo-inverse of Θ_X . To promote the sparsity of the matrix Ξ , a threshold λ is introduced. For the j th column ξ_j^0 in Ξ^0 , the indices for the values which are greater than λ are recorded in the j th column S_j^{new} of the index matrix S^{new} . Then the least square fit will perform only for the elements with indices in S_j^{new} in the new iterations to get ξ_j^{new} (S_j^{new}). The process is repeated until the index matrix S remains the same between two iterations or the maximum iteration number is met. The pseudo code is presented in Algorithm 1.

It has been proved in [15] that SINDy algorithm approximates the local minimizer of the non-convex objective function with the zero norm penalty term as the following:

$$F(\Xi) = \left\| \Theta_X \Xi - \dot{X} \right\|_2^2 + \lambda^2 \|\Xi\|_0 \quad (21)$$

To see that, after each iteration, the element of Ξ is either with a least square solution that is greater than λ or zero, implying that the number of iterations for SINDy algorithm to converge is finite and at most equals to the cardinality of Ξ^0 , i.e., $card(\Xi^0)$. Additionally, in the application of power systems, some elements of Ξ are known to be zero as derived from power system physical model (see (17)-(19)), those parts are enforced to be zero during the regression process.

If forced oscillations are detected, for example, from modal oscillation component properties and envelope shapes by [31]–[33], their sources can be further located from index ζ which can be calculated from the estimated Ξ_{ab} :

$$\zeta_{ij} = a_{ij}^2 + b_{ij}^2 \quad i \in \{1, \dots, n\}, j \in \{1, \dots, r\} \quad (22)$$

From (2), it can be seen that ζ_{ij} is the estimated magnitude squared of the injected forced oscillation of frequency ω_{F_i} at generator j . Therefore, the forced oscillation frequencies ω_{F_i} and the source generators j can be identified from the peak values in $\{\zeta\}$. Due to the sparsity of ζ matrix, outlier selection algorithms can be applied to pinpoint the peaks. An outlier is defined as a value that is more than three scaled Median Absolute Deviations (MAD) away from the median [34]. In particular, function “isoutlier” in Matlab® R2019 can be applied to detect the forced oscillation frequencies and their sources.

Algorithm 1: The Sequential Thresholded Least-Square Sparse Regression

Input: $\Theta_X, \dot{X}, \lambda$
Output: Ξ^{new}

Initialize: $\begin{cases} iter \leftarrow 1 \\ \Xi^{old} \leftarrow \Xi^0 = \Theta_X^\dagger \dot{X} \\ S^{old} \leftarrow 0_{2r \times (1+2r+2n)} \end{cases}$

- 1 **while** $iter < card(\Xi^0)$ **do**
- 2 **for** $j \leftarrow 1$ **to** $2r$ **do**
- 3 $S_j^{new} = \begin{cases} 1, & \text{if } \left\{ \xi_j^{old} \right\} \geq \lambda \\ 0, & \text{if } \left\{ \xi_j^{old} \right\} < \lambda \end{cases}$
- 4 $\xi_j^{new} (S_j^{new}) = \Theta \left(:, S_j^{new} \right)^\dagger \dot{X}(:, j)$
- 5 **if** $S_j^{new} \neq S_j^{old}$ **then**
- 6 $S_j^{old} \leftarrow S_j^{new};$
- 7 $iter ++;$
- 8 **else**
- 9 **break;**

Assuming a forced oscillation event is detected, the flow chart of the proposed algorithm in locating forced oscillations is summarized in Fig. 1, followed by some important remarks.

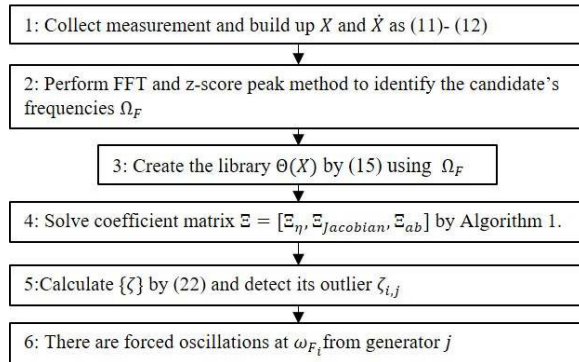


Fig. 1: The flow chart of the proposed algorithm of locating forced oscillations.

Remarks:

- In Step 1, $m = 1200$ is used for most of the cases in the library [19] i.e., 40s PMU data with a sampling frequency of 30 Hz, except for Cases 4 and 5 in the actual oscillation events in ISO-NE system where 80s PMU data is used due to weak oscillation magnitudes. The applied sample size ensures that the forced oscillation frequencies can be captured accurately. The computational time of the proposed algorithm is approximately 3 seconds for all cases using Matlab[®] R2019 software on Intel i7-7700HQ CPU with 16GB RAM computer, which demonstrates a good feasibility of the proposed algorithm in online applications.
- The proposed method requests the derivatives of frequencies. Although Rate Of Change Of Frequency (ROCOF) is standard measured data [35], it may be unavailable or inaccurate in practice. A numerical finite difference method, specifically,

the two-points forward difference approximation method [36] is applied to estimate the derivatives of frequencies in the simulation studies of this paper if they are not available. In practice, the frequency measurement filter proposed in [37] or the frequency estimation algorithm using the point-on-wave model in [38] may further enhance the measurement accuracy and improve the performance of the proposed method.

- In this paper, FFT is applied to identify forced oscillation frequency candidates. Goertzel algorithm and Welch's method can also be applied as alternatives for a higher resolution spectrum. Since FFT, Goertzel and Welch algorithms can provide good candidate sets in all the numerical studies presented in Section V-VI, we only present the results using FFT.

- If the forced oscillation sources are outside the study area, the border bus treated as an aggregation of the external area may be identified as the source by the proposed algorithm as shown in Section VI-C. Further effort is needed to extend the method to investigate the situations in which the forced oscillation sources are not generators.

- In all cases presented in Section V-VI, λ is selected as 10^{-6} that gives an expected sparsity level for Ξ_{ab} ($> 50\%$, see (16)-(19)). In practice, the value of λ may need to be adjusted in different systems and can be determined considering the expected sparsity level of Ξ_{ab} . Besides, the sparse promoting process for the thresholded Least absolute Shrinkage and Selection Operator (thresholded LASSO) [39] can also be used to promote the non-zero coefficients in the proposed algorithm without the need of selecting λ .

V. TESTING IN SIMULATED CASES

In this section, the performance of the proposed algorithm of locating forced oscillations is tested in all 24 cases available in the IEEE Task Force test cases library [18], [19]. In all cases, all natural modes are reasonably damped with damping ratios higher than 5%. The test results of the proposed algorithm in the IEEE 68-bus system and the WECC 240-bus system are also presented. It will be shown that the proposed method can successfully detect forced oscillations sources even when the system is under resonance condition (i.e., the forcing frequency overlaps with a natural mode).

A. Case A: One Forced Signal, Resonance with an Inter-Area Mode

One challenging situation for any forced oscillation locating method is when resonance occurs such that large magnitude oscillations are observed in multiple locations. In light of this, we test the performance of the proposed algorithm under resonance conditions. Particularly, we take Case *F3* in the forced oscillation simulated test case library [18] as an example, which is also available online [19]. The performance of the proposed method in all 18 simulated cases is also presented in Table I. The library dataset is produced by TSAT software from simulation of WECC 179-bus system.

In Case *F3*, forced oscillation is injected into the excitation system as a sinusoidal signal at the generator at bus 77 with a frequency 0.37Hz to cause resonance with the inter-area 0.37 Hz mode. More details can be found in [19]. The trajectories of frequencies are presented in Fig. 2 (a). The largest oscillation

amplitude in frequency is observed at the generator at bus 65 (marked by bold green) rather than the actual source, i.e., the generator at bus 77 (marked by bold blue).

Following the proposed algorithm, 40s, 30Hz emulated rotor angles and frequencies are used to build up the measurement matrix X and \dot{X} . The finite difference method is applied to estimate \dot{X} . In Step 2, the FFT and the z-score peak detection method are applied to detect the peak oscillation frequencies. As seen from the single-sided amplitude spectrum in Fig. 2 (b), natural frequencies and forced oscillation frequencies are mixed. After removing 26 duplication, 3 candidate frequencies are collected in Ω_F as presented in Fig. 2. (c). Particularly, 0.37 Hz, the true forced oscillation frequency is identified, which overlaps with a natural inter-area mode.

Next, the feature library $\Theta(X)$ is built in Step 3 using 3 candidate frequencies. The coefficient matrix $\Xi = [\Xi_\eta, \Xi_{\text{Jacobian}}, \Xi_{ab}]$ is further obtained in Step 4. Particularly, Ξ_{ab} corresponding to the forced oscillation terms is shown in Fig. 3 (a), from which it can be evidently seen that there is one peak term at 0.37 Hz.

Following the proposed algorithm, the indexes $\{\zeta\}$ are calculated and the outliers are detected, as shown in Fig. 3 (b)-(c). It is determined by the proposed algorithm that there is one oscillation source, i.e., the generator at bus 77, at a frequency of 0.37 Hz, which well agrees with the description of the source for this case in the test library. In addition, it takes only 3.07 seconds for locating, showing a high computational efficiency of the proposed method.

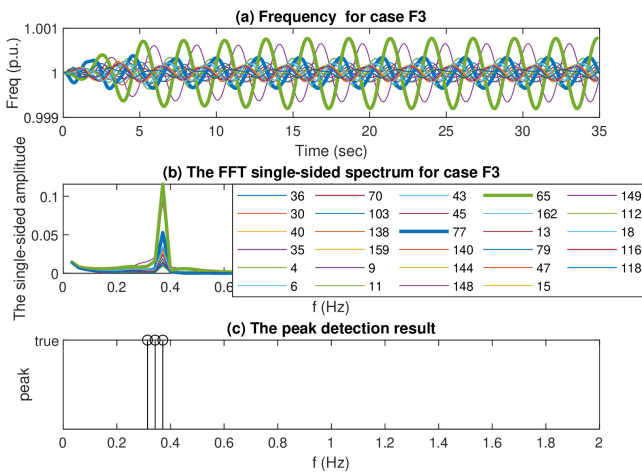


Fig. 2: (a). The trajectories of rotor frequencies; (b) The single-sided spectrum from FFT; (c) The peak frequencies detected for Case A (Case $F3$ in [19]).

B. Case B: Under a Rectangular Forced Oscillation

In Case $FM6 - 2$ [19], forced oscillation is injected into governor as a rectangular and symmetric signal at the generator at bus 79. The forced signal creates the spectrum of odd harmonics 0.2, 0.6, 1.0, 1.4 Hz, etc. with the lowest frequency 0.2 Hz [19]. The trajectories of frequencies are presented in Fig. 4 (a), showing that the signal of the source (marked in bold blue) does not have the largest oscillation magnitude.

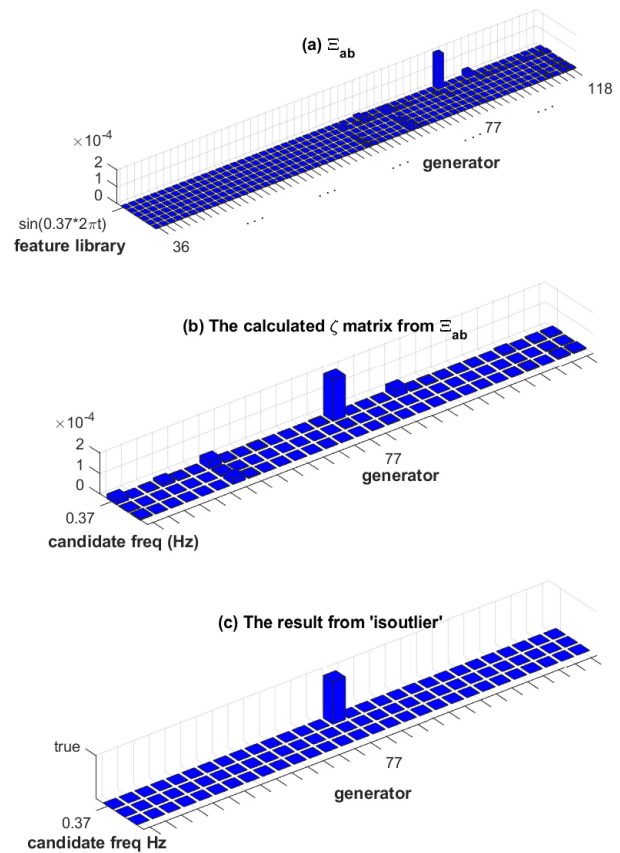


Fig. 3: (a) Ξ_{ab} , (b) ζ , and (c) outliers of ζ for Case A (Case $F3$ in [19]).

Similarly, 40s, 30Hz emulated rotor angles and frequencies are used by the proposed algorithm. The FFT and the z-score peak detection method for the trajectories are presented in Fig. 4 (b)-(c). After removing 26 duplication, 2 candidate frequencies are collected in Ω_F as presented in Fig. 4. (c). The indexes $\{\zeta\}$ are calculated and the outliers are detected. As shown in Fig. 5 (left) and (right), the generator at bus 79 is detected to be the source of the oscillation, which agrees with the description. The processing time for locating is 3.04 seconds.

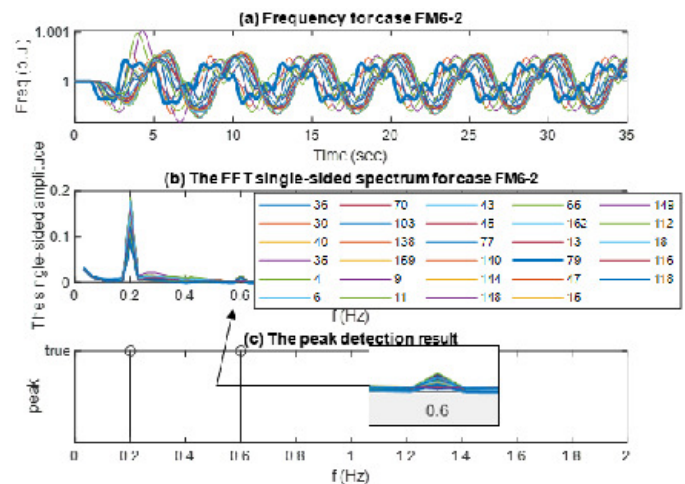


Fig. 4: (a). The trajectories of rotor frequencies; (b) The single-sided spectrum from FFT; (c) The peak frequencies detected for Case B (Case $FM6 - 2$ in [19]).

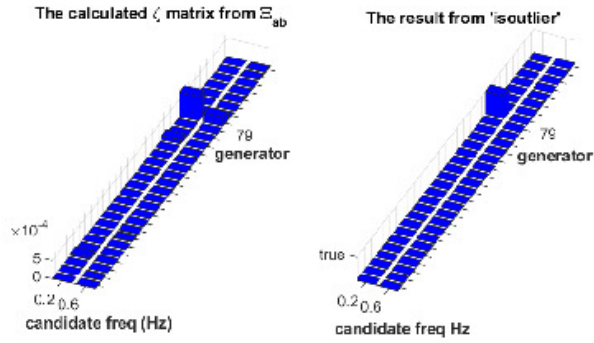


Fig. 5: ζ (left) and outlier (right) result for Case B (Case $FM6 - 2$ in [19]).

For comparison, the RPCA method proposed in [11] was implemented using the same measurements. Leveraging on the sparsity of the forced oscillation sources along with the low-rank nature of rotor dynamics, the RPCA method computes the sparse and low-rank components of the measurement matrix and detects the forced oscillation sources by finding the largest absolute value in the sparse residual matrix S . The sparse residual matrix S and its row maximum absolute values calculated by the RPCA method are shown in Fig. 6, from which it can be seen that the maximum absolute value of S has a row index corresponding to bus 35. Thus, the RPCA method regards the generator at bus 35 to be the source, failing to pinpoint the right source, i.e., the generator at bus 79.

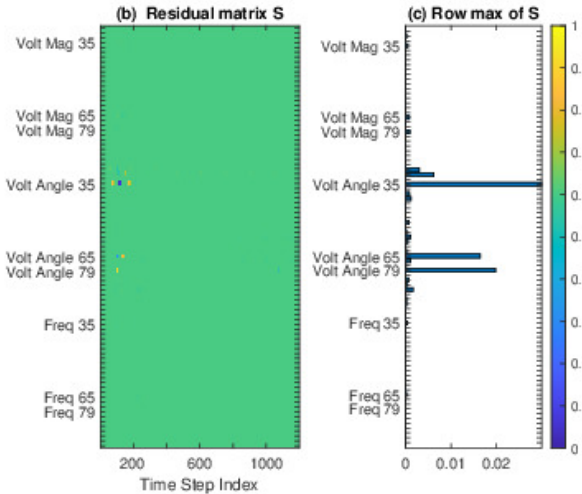


Fig. 6: Visualization of the sparse residual matrix S by the RPCA method (left) and the maximum absolute value in each row of S (right) Case B (Case $FM6 - 2$ in [19]).

C. Case C: Two Sources of Forced Signals, Resonance with Two Modes

In Case $FM7 - 1$ [19], two forced sinusoidal signals with fundamental frequencies 0.65Hz and 0.43Hz are injected into the governors of generators at bus 79 and that at bus 118, respectively, which are very close to two inter-area modes 0.667 Hz and 0.445 Hz. The trajectories of frequencies are presented in Fig. 7 (a), in which the source trajectories are marked in bold blue and light green. Again, the oscillations

at the sources do not have the largest amplitudes among all frequency measurements, which is a typical sign of resonance as discussed in [9] [11]. After removing 80 duplication, 9 candidate frequencies containing both forced oscillation frequencies and natural modes are collected in Ω_F as presented in Fig. 7 (c). Again, the indexes $\{\zeta\}$ are calculated and the outliers are detected. As shown in Fig. 8, the generators at bus 79 and bus 118 are pinpointed as the oscillation sources, which agree with the description from the test case. It is worth noting that there are no peaks/outliers detected at the natural oscillation frequencies, even though the forced oscillation frequencies are very close to the natural ones. The processing time for locating the sources is 3.4 seconds.

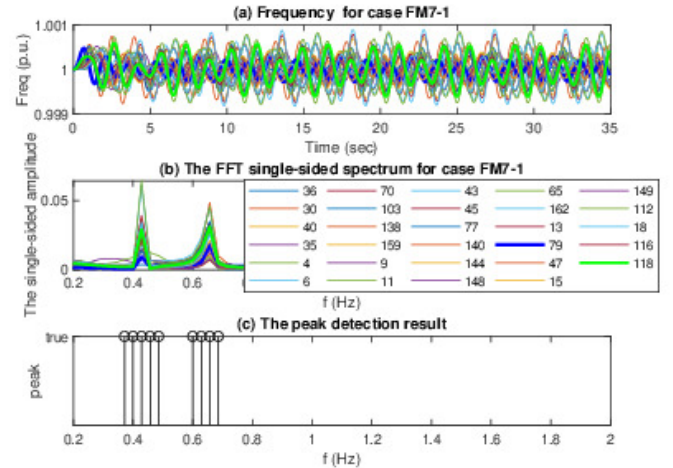


Fig. 7: (a). The trajectories of rotor frequencies; (b) The single-sided spectrum from FFT ; (c) The peak frequencies detected for Case C (Case $FM7 - 1$ in [19]).

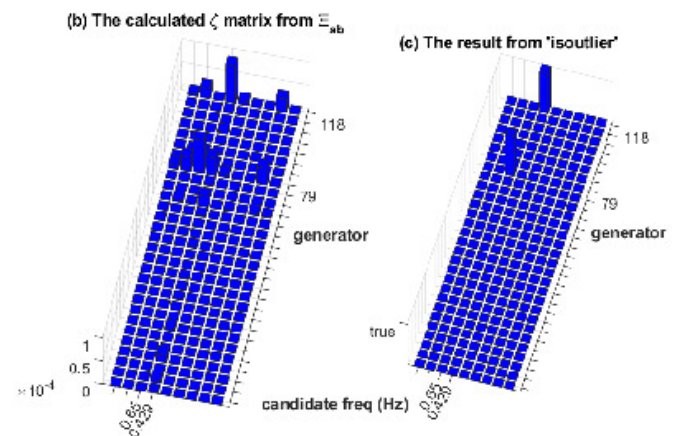


Fig. 8: ζ (left) and outlier (right) result for Case C (Case $FM7 - 1$ in [19]).

For comparison, the results of RPCA method using the same measurements are presented in Fig. 9. The row index of the maximum absolute value of the sparse residual matrix S corresponds to the generator at bus 79. However, the other

source, i.e., the generator at bus 118, is missed. Note that the RPCA method in [11] detects the forced oscillation source by observing the maximum absolute value of S and thus is intrinsically unable to handle the cases with multiple forced oscillation sources. Moreover, the component corresponding to the true source, the generator at bus 118, does not even rank high in terms of absolute value as seen in Fig. 9 (right).

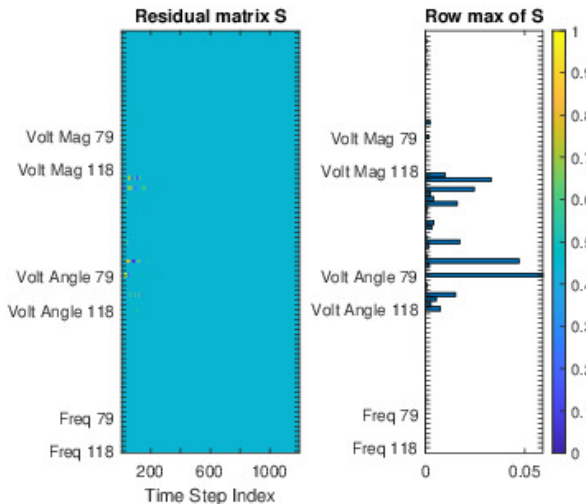


Fig. 9: Visualization of the sparse residual matrix S by the RPCA method (left) and the maximum absolute value in each row of S (right) for Case C (Case $FM7-1$ in [19]).

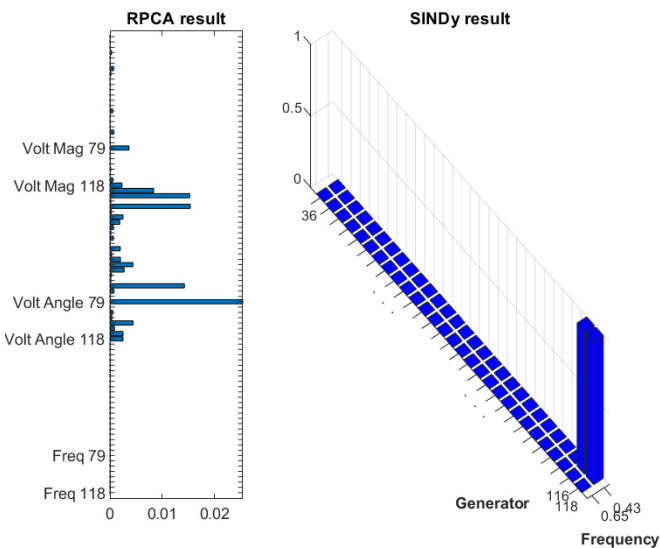


Fig. 10: Visualization of the RPCA result (left) and SINDy result (right) comparison for Case $F7-1$ in [19].

In addition, the proposed algorithm and the RPCA method [31] are tested for all 18 simulated cases available in the test case library [19]. As presented in Table I, both the proposed algorithm and the RPCA method are successful in most cases. However, the proposed algorithm fails in Case $F7-1$, while the RPCA method fails in Case $F7-1$, Case $FM6-2$ (Case B), and Case $FM7-1$ (Case C).

In Case $F7-1$, two sinusoidal forced oscillations are injected into the excitation systems of the generator at bus 79 and that at bus 118, respectively, to cause resonances with two different modes at frequencies 0.65 Hz and 0.43 Hz. Particularly, the oscillation magnitude of the 0.65 Hz forced signal injected to the excitation system of the generator at 79 is only 0.006 p.u, a very small magnitude. As shown in Fig. 10, the proposed algorithm fails to capture the oscillation of 0.65 Hz and its source at bus 79, while captures the oscillation of 0.43 Hz and its source, though both the generator at bus 116 and that at bus 118 are picked. On the other hand, the RPCA method fails to capture the source of the forced oscillation at 0.43 Hz while correctly pinpoints the source of the oscillation at 0.65 Hz, i.e., the generator at bus 79.

Based on the results in Table I, another observation found through the analysis is that compared to the RPCA method, the proposed algorithm may perform better in cases where the forced oscillations come from the governor compared to the RPCA method. The reason is that the proposed algorithm is based on the swing equations in which the forced signal is assumed to affect the mechanical power (see (1)) that is typically controlled by the turbine governor. Yet, the RPCA method does not assume any physical model and seems to perform less robust in these cases (e.g., FM cases in Table I).

D. Case D: Forced Oscillation with a Sudden Frequency Change

To test the performance of the proposed method when the forcing frequency suddenly changes, we conducted some simulations in the IEEE 68-bus system using Power System Analysis Toolbox (PSAT) simulation software [40] as the library [19] does not contain such a case. In the IEEE 68-bus system, 16 generators are modelled by the fourth-order model equipped with the standard IEEE type 1 automatic voltage control regulators (AVRs). Generator 1 is selected as the reference generator. The standard deviation of load fluctuation is set to 1 (σ_{load_i} in (4)). The proposed algorithm uses the first 40s emulated PMU measurements of rotor angles and frequencies of Generator 2-16 with a sampling rate of 60 Hz to build the measurement matrix X and \tilde{X} . At the beginning, the forced oscillation with a frequency of 0.24 Hz and a peak strength of 5% of the mechanical power input is injected into Generator 12. Later at 20s, the forced oscillation suddenly switches to 0.27 Hz with a peak strength of 10% of the mechanical power input. The trajectories of rotor frequencies is presented in Fig. 11 (a). The single-sided amplitude spectrum for the trajectories is shown in Fig. 11 (b). After removing 63 duplication, 6 candidate frequencies are collected from peak detection process in Ω_F including 0.25 Hz and 0.275 Hz that are close to the true forcing frequencies as shown in Fig. 11 (c).

It is determined by the proposed algorithm that there is forced oscillation from Generator 12 at 0.25 Hz as shown in Fig. 14 (right). However, since there is a sudden change of forcing frequency, the calculated ζ matrix has peaks at both 0.25 Hz and 0.275 Hz as shown in Fig. 14 (left), indicating a potential change of frequency in the time window applied.

TABLE I: Single location cases with resonance between forced oscillation and system modes from [18]

Case prefix "F" and "FM" is for FO in the excitation and governor system		SINDy Result			RPCA Result
Cases Name	Description	Source bus	Est Source bus	Est Freq	Est Source bus
F1	Resonance with local 0.86Hz mode	4	4	0.86	4
F2	Resonance with local 0.86Hz mode	79	79	0.86	79
F3	Resonance with inter-area 0.37Hz mode	77	77	0.36	77
F4-1	Below natural 0.84Hz mode	79	79	0.8	79
F4-2	Between natural 0.84Hz and 0.86Hz modes	79	79	0.86	79
F4-3	Higher than natural 0.86Hz mode	79	79	0.9	79
F5-1	Below natural 0.44Hz inter-area mode	79	79	0.42	79
F5-2	Between natural 0.44Hz and 0.47Hz inter-area modes	79	79	0.46	79
F5-3	Higher than natural 0.47Hz inter-area mode	79	79	0.5	79
F6-1	Rectangular wave of 0.1Hz	79	79	0.3	79
F6-2	Rectangular wave of 0.2Hz	79	79	0.2	79
F6-3	Rectangular wave of 0.4Hz	79	79	0.8	79
F7-1	Two resonance modes 0.65 Hz (bus 79) and 0.43 Hz (bus 118)	79,118	116,118	both at 0.43	79
F7-2	Two signals resonance with same mode 0.43 Hz	70,118	70,118	both at 0.43	65
FM1	Resonance with local 0.86Hz mode	4	4	0.86	4
FM3	Resonance with inter-area 0.37Hz mode	77	77	0.37	77
FM6-2	Rectangular wave of 0.2Hz	79	79	0.2	35
FM7-1	Two resonance modes 0.65 Hz (bus 79) and 0.43 Hz (bus 118)	79,118	79,118	0.657 Hz (bus 79) 0.43 Hz (bus 118)	79

Nevertheless, the source Generator 12 is located correctly by the proposed method.

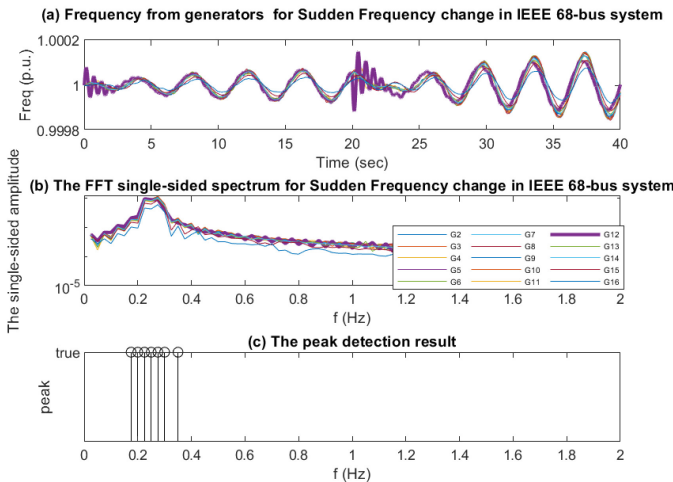


Fig. 11: (a). The trajectories of rotor frequencies; (b) The single-sided spectrum from FFT ; (c) The peak frequencies detected for Case D (forced oscillation with a sudden frequency change at 20s).

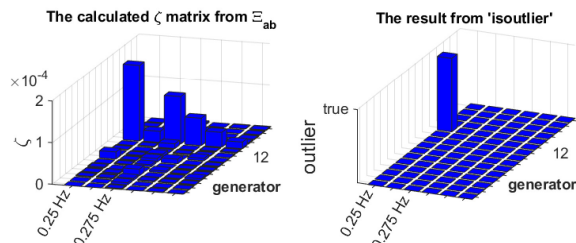


Fig. 12: ζ (left) and outlier (right) result for Case D (forced oscillation with a sudden frequency change at 20s).

E. Case E: Under Load Power Factor Variation

Although constant power factor is assumed in (4), it may not be true in practical applications. To test the performance of the proposed method under load power factor variation, some simulations in the IEEE 68-bus system were carried out in PSAT. The generators and their control set up are the same as in Section V-D. In addition, all 34 loads in the system have been replaced by voltage dependent loads. The active and reactive power of the dynamic loads are set as random variables following normal distributions with standard deviations equal to 0.01% of their original power flow solutions. If the random load changes cause the power factor falls below 0.95 any time in the simulation, the reactive power will be adjusted accordingly to maintain 0.95 power factor, mimicking the power factor correction action.

Similar to Section V-D, we assume that the forced oscillation of 0.25 Hz (near the system mode 0.243 Hz) is injected into the system through the mechanical power of Generator 12 with a peak strength of 5% of the mechanical power output. Fig. 13 (top) shows that the voltage magnitudes are varying randomly due to the variations of both active and reactive power (i.e., power factors). The trajectories of rotor angles and frequencies are presented in Fig. 13 (mid) and (bottom). The proposed algorithm uses 40s, 60 Hz emulated rotor angles and frequencies of Generator 2-16 to build the measurement matrix X and \hat{X} . Likewise, the finite difference method is applied to estimate $\Delta\omega_i(t)$. It can be seen from Fig. 14 (right) that the proposed method can determine accurately that the forced oscillation is from Generator 12. The results align well with the simulation setup. From the simulation results, we observe that the proposed algorithm is capable of working under small power factor variations.

F. Case F: Testing with sixth-order generator models in the WECC 240-bus system

For further validation, we carried out simulations in the WECC 240-bus system in TSAT software [41], which was

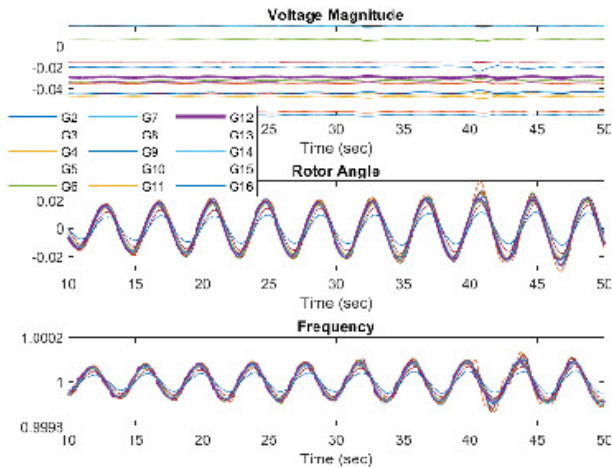


Fig. 13: The trajectories of voltage magnitudes (top), rotor angles (mid), and rotor frequencies (bottom) for Case E (under load power factor variations).

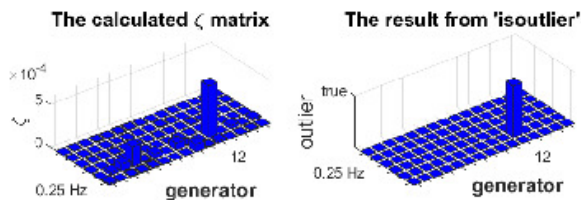


Fig. 14: ζ (left) and outlier (right) result for Case E (under load power factor variations).

developed by National Renewable Energy Laboratory (NREL) [42]. The system has 243 buses, 146 generating units at 56 power plants. All synchronous generators are modelled as the sixth-order GENROU synchronous generator model. The small-signal analysis result can be found [43]. The forced oscillations with the peak strength of 40MW are injected into the system through the TGOV1 governor models or SEXS excitation models. The forced oscillation frequencies are set at the exact mode frequencies, aiming to create resonance cases. Three system mode frequencies at 1.1819 Hz, 0.803 Hz and 0.5774 Hz are picked, the damping ratios of which are 4.5%, 6.5%, and 8.1%, respectively. Additional cases with the rectangular forced signal with a fundamental frequency of 0.37Hz are also tested. 11 generators are randomly selected from different areas for the injection of forced oscillations. The largest oscillation amplitudes appear at non-source buses in all cases except the cases involving buses 2634, 6335, or 7031. The proposed algorithm successfully locates the source bus for all cases. The summary of the test results is shown in

Table II.

TABLE II: Result summary for tests in WECC 240-bus

Simulation setup		SINDy Result	
Source	Description	Source	Freq(Hz)
1034	Sine wave of 0.5774Hz from exciter	1034	0.577
1431	Sine wave of 0.803Hz from governor	1431	0.803
2634	Sine wave of 1.1819Hz from governor	2634	1.18
3933	Sine wave of 0.5774Hz from exciter	3933	0.577
4132	Sine wave of 0.803Hz from governor	4132	0.803
5032	Sine wave of 1.1819Hz from exciter	5032	1.18
6533	Sine wave of 0.5774Hz from governor	6533	0.577
7031	Sine wave of 0.803Hz from exciter	7031	0.803
7032	Sine wave of 1.1819Hz from governor	7032	1.18
2030	Rectangular wave of 0.37Hz from exciter	2030	0.74
6335	Rectangular wave of 0.37Hz from governor	6335	0.37

VI. TESTING IN ACTUAL OSCILLATION EVENTS

In the next three subsections, the performance of the proposed algorithm is tested using the measurements from the real-life forced oscillation events in the system of ISO-NE [19]. The partial map for the system is shown in Fig. 15. There are three generators inside the study area: G1 (Gen1 at Substation 6), G2 (Gen2 at Substation 7), and G3 (Gen 1 at Substation 8). The study area is connected to two external areas “Area 2” and “Area 3”. In addition, the boundary buses—Line 7 at Substation 3 (Ln:7) and Line 21 at Substation 9 (Ln:21)—are used to represent aggregations of external areas. As rotor angles are unavailable, the measurements of voltage angles and frequencies of all generator substation terminal buses and the aforementioned two boundary buses are used. Such change may affect the estimation of the Jacobian matrix, but the coefficient matrix Ξ_{ab} still preserves the information of forced oscillation. The bus—Line 11 at Substation 5 (Ln:11) is chosen as the reference bus. The raw PMU data are fed directly to the proposed algorithm.

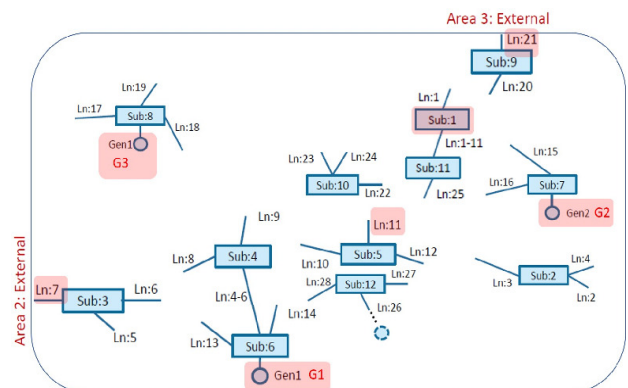


Fig. 15: Partial map for ISO New England system from [19].

Moreover, the success of the proposed method using data from actual oscillation events demonstrates its robustness with respect to measurement noise, general drift of measurements, and other imperfections in practical applications. In the end, we will also discuss the limitations of the proposed algorithm.

A. ISO-NE Case 3 in [19]: an Actual Forced Oscillation Event With Strong Forcing Strength

The first forced oscillation event (ISO-NE Case 3 in [19]) under study occurred on July 20th, 2017. It was a regional oscillation event. The modes were widely observed within the system. The peak-to-peak magnitude of the oscillation reached 115 MW with a peak load of about 26,000 MW. The oscillation frequency was 1.13 Hz. The source of the oscillation was close to G2. Fig. 16 (a)-(b) present 40s measurements of voltage angles and frequencies of all generators' terminal buses fed to the proposed algorithm. The single-sided spectrum of all measurements obtained from the FFT are presented in Fig. 16 (c). Fig. 16 (d) shows the 7 candidate frequencies identified.

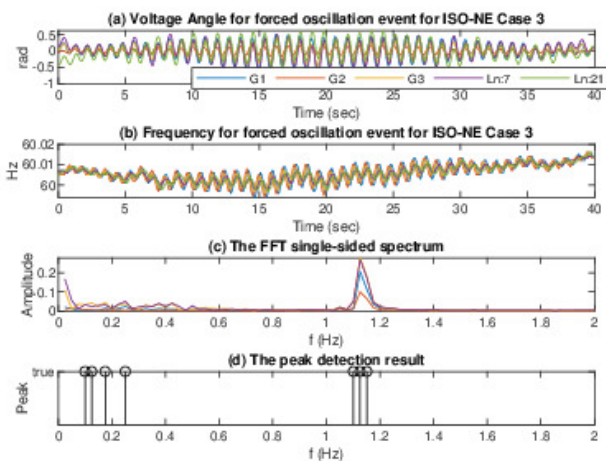


Fig. 16: (a). The trajectories of voltage angles; (b) The trajectories of voltage frequencies; (c) The single-sided spectrum from FFT; (d) The peak frequencies detected for ISO-NE Case 3 in [19].

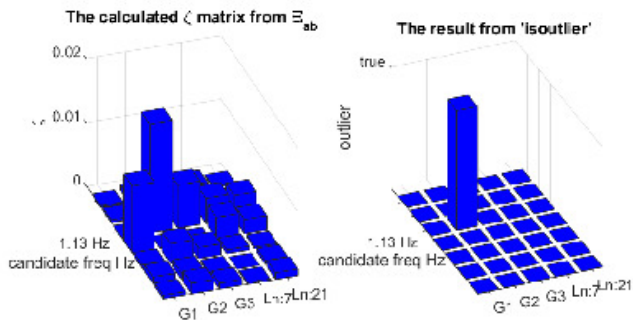


Fig. 17: ζ (left) and outlier (right) result for ISO-NE Case 3 in [19].

Next, the coefficient matrix Ξ is estimated. The indexes $\{\zeta\}$ are calculated and the outliers are identified as presented in Fig. 17, in which a spike appears. It indicates that there is a forced oscillation at 1.13 Hz from G2. The results well align with the identified cause of this event mentioned above, showing that the proposed algorithm can successfully locate

the source in practical applications despite measurement noise, general drift of the data, etc. Furthermore, the algorithm takes only 1.77s for the whole process. In contrast, the RPCA method identifies the bus—Line 21 at Substation 9 (Ln:21) as the source, which is unfortunately incorrect.

B. ISO-NE Case 5 in [19]: an Actual Forced Oscillation Event With Low Forcing Strength

Another case we studied was the forced oscillation event in the system of ISO-NE on January 29th, 2018 (ISO-NE Case 5 in [19]). Again, the oscillation was caused by G2. However, the peak-to-peak magnitude was 15 MW, much smaller than that in the previous case. The forced oscillation frequency was around 1.587 Hz with a potential graduate frequency variation between 1.57 Hz and 1.63 Hz.

As the oscillation magnitude is small, measurements of 80s rather than the default 40s used in previous cases of voltage angles and frequencies of all generators' terminal buses are used to capture the forced oscillation frequency candidates. As shown in Fig. 18 (a)-(b), the forced oscillations can be hardly observed in the time-domain plots. Fig. 18 (c) presents the single-sided spectrum obtained from the FFT. With the help of the z-score peak detection method, 23 candidate frequencies are identified as shown in Fig. 18 (d).

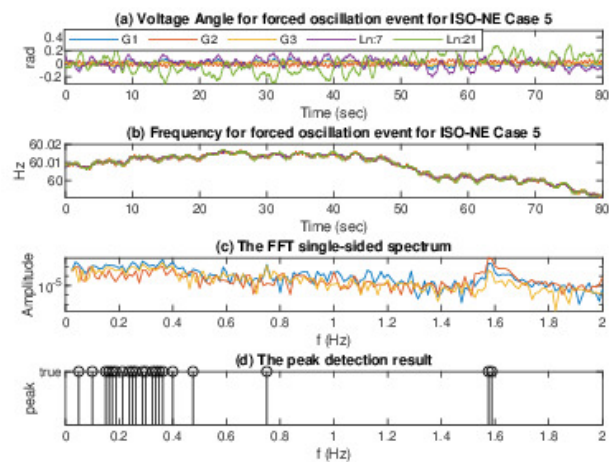


Fig. 18: (a). The trajectories of voltage angle; (b) The trajectories of voltage frequencies; (c) The single-sided spectrum from FFT; (d) The peak frequencies detected for ISO-NE Case 5 in [19].

The indexes $\{\zeta\}$ are further calculated as well as the outliers, as presented in Fig. 19. The results imply that there is a forced oscillation at 1.59 Hz from G2, well consistent with the identified cause. Moreover, the algorithm takes only 2.08s for the whole process.

C. Further Validations of the Proposed Method in Actual Forced Oscillation Events

In this section, the other cases (Case 1, 2, 4 and 6 in ISO-NE) available in the library [19] are tested, in which the source is outside the study area or there are missing measurements.

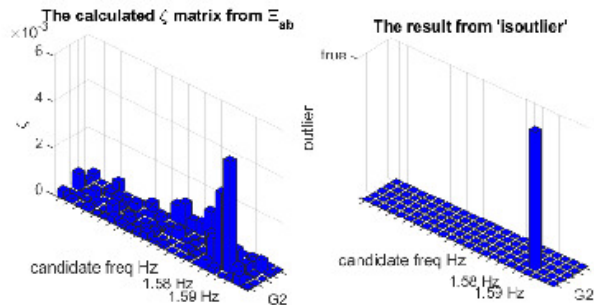


Fig. 19: ζ (left) and outlier (right) result for ISO-NE Case 5 in [19].

In Case 1 and 4, the forced oscillation source is in the external Area 2. Case 1 occurred on June 17th, 2016, with a peak-to-peak magnitude up to 27 MW. Case 4 occurred on Feb. 14th, 2018, with a peak-to-peak magnitude up to 10 MW. Both the proposed algorithm and the RPCA method identify that the border bus of Area 2—Line 7 at Substation 3 (Ln:7) is the source.

In Case 2, the data from G1 and G3 is missing. In fact, all measurements of Substation 6 and Substation 8 are unavailable. Case 2 occurred on October 3rd, 2017, with a peak-to-peak magnitude up to 130 MW. To apply the proposed algorithm, the data from Line 4-6 at Substation 4 that is a direct connection to Substation 6 is used to replace $G1$, while the channel for $G3$ has to be dropped. The proposed algorithm declares Line 21 at Substation 9 as the source, indicating that the forced oscillation may be from Area 3, which is consistent with the identified cause. The RPCA method also correctly pinpoints the source in this case.

The results of the proposed algorithm and the RPCA method for all actual oscillatory events from [19] are summarized in Table III. It is observed that SINDy is able to accurately identify the sources in most cases except Case 6 in which the forced oscillations can be hardly observed in any voltage angle measurements. Case 6 occurred on June 20th, 2019, with peak to peak magnitude up to 9 MW. The PMU measurements are obtained from 4 transmission lines connected to Substation 1 (though only two lines are marked on the map in Fig. 15 [19]). Unfortunately, the proposed algorithm cannot establish a relationship between the voltage angles and bus frequencies, leading to a regularized result (all elements are non-zero and equally high) in Ξ_{ab} . Therefore, the source is not located. This indicates that it might be insufficient to use classic swing equation to describe the voltage angle and frequency relationship for a bus not directly connected to a generator, especially when the generators are far away from the bus or when the forced oscillation magnitude is small. Or more advanced signal processing techniques are needed to remove all the environmental noise and reappear the forced oscillation signals in the trajectories. Besides, further efforts need to be devoted to searching for more appropriate nonlinear relationships used by SINDy when the measurements are far away from generators or when the forced oscillation sources are not generators (e.g., HVDC control).

VII. COMPARISON WITH THE DISSIPATING ENERGY FLOW METHOD

The energy flow based forced oscillation locating method is widely used in the utility practice, which is accurate and robust [13]. In this section, we show that the proposed SINDy algorithm can be a valuable companion to the energy-based method in some tricky cases. Similar to the approach in [11], we assume that the measurements of the source generator at bus 4 are not available, while the measurements of all the other generators are available. The results from the the Dissipating Energy Flow method (DEF) in [44], the proposed SINDy, and the RPCA are presented in Fig. 21, respectively. Both the RPCA and the proposed SINDy algorithm suggest that the sources are the generators at bus 9 and bus 18 as shown in Fig. 21 (bottom left and bottom right). In addition, bus 30 is also among the top three elements in the residual matrix in the RPCA method as shown in Fig. 21 (bottom left). In contrast, the DEF method fails to identify the source as there are no dissipating energy flows from the generator buses to the network (all energy curves near or lower than zero in Fig. 21 (top)). The full result summary for the DEF, the RPCA and the proposed SINDy is shown in Table IV, showing that the proposed SINDy algorithm may complement the DEF method when the measurements of the true source are unavailable.

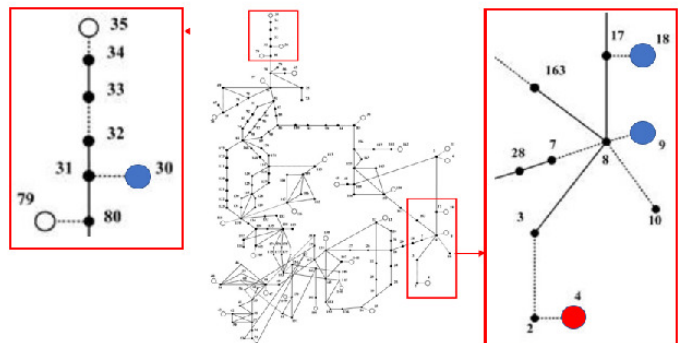


Fig. 20: Map for WECC 179-bus power system used for Case FM1 with no source measurement result [19].

VIII. CONCLUSION AND FUTURE WORK

In this paper, a purely data-driven algorithm for forced oscillation location has been proposed. Leveraging on the sparse identification for nonlinear dynamical system, the proposed algorithm can extract the dynamics of a power system from PMU data to locate forced oscillation sources. The proposed algorithm is evaluated with good results using the simulated cases and actual oscillation events available in the IEEE Task Force test cases library as well as in the simulated IEEE 68-bus system. Future developments such as developing an effective feature library when forced oscillation sources are not generators are needed.

APPENDIX A

REPRESENTING FORCED OSCILLATIONS FROM EXCITERS AND TURBINE GOVERNORS IN SWING EQUATIONS

TABLE III: Cases of actual oscillatory events from [19]

Real events		SINDy Result		RPCA Result	
ISO-NE	Description	Real Location	Est Location	Est Freq (Hz)	Est Location
Case 1	Near-resonance conditions with natural oscillatory mode 0.27 Hz	Ln:7 (Area 2)	Ln:7	0.275, 0.286	Ln:7
Case 2	Growing oscillations at 0.08Hz, 0.15Hz and 0.31Hz	Ln:21 (Area 3)	Ln:21	0.338	Ln:21
Case 3	Equipment issue in generator 2 has created 1.13	G2	G2	1.13	Ln:21
Case 4	Possible resonance case with 0.25Hz mode	Ln:7 (Area 2)	Ln:7	0.25	Ln:7
Case 5	Local oscillations caused by generator 2	G2	G2	1.59	G2
Case 6	PMU measurements from Substation 1 transmission line 1 to 4	Substation 1 Ln:2	Cannot tell	0.0107	Sub1 Ln:2

TABLE IV: Result summary for cases *FM1* with special conditions

Case Description	DEF Result	RPCA Result	SINDy Result
No measurements from source bus 4, PMUs are installed only in generator bus, 9 and 18 are the closest generator buses	Cannot tell	Bus 30, 9, and 18	Bus 9, and 18

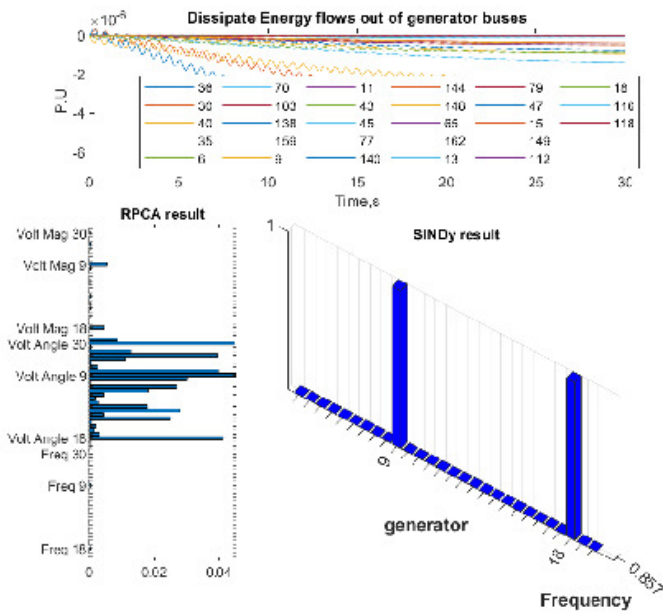


Fig. 21: Result for Dissipating energy flow (DEF) (top), RPCA (bottom left), and SINDy (bottom right) of all generators except the source bus 4 in case *FM1* with no source measurement.

As discussed in [9], the linearized rotor dynamics for a single machine connected to an infinite bus can be represented as below:

$$\begin{aligned}
 \begin{bmatrix} \Delta \dot{\delta} \\ \Delta \dot{\omega} \end{bmatrix} &= \begin{bmatrix} 0 & 1 \\ -\frac{V_t E'}{M X_d'} \cos(\varphi) & -\frac{D}{M} \end{bmatrix} \begin{bmatrix} \Delta \delta \\ \Delta \omega \end{bmatrix} \\
 &+ \begin{bmatrix} 0 & 0 \\ -\frac{E'}{M X_d'} \sin(\varphi) & \frac{V_t E'}{M X_d'} \cos(\varphi) \end{bmatrix} \begin{bmatrix} \Delta V_t \\ \Delta \theta_t \end{bmatrix} \\
 &+ \begin{bmatrix} 0 \\ \frac{1}{M} \end{bmatrix} [\Delta P_m] + \begin{bmatrix} 0 \\ -\frac{V_t}{M X_d'} \sin(\varphi) \end{bmatrix} [\Delta E']
 \end{aligned} \quad (23)$$

where δ and ω is rotor angle and frequency; M and D are the inertia constant of the generator and the damping coefficient of the generator; V_t and E' denote the terminal voltage and the generator internal electromotive force (emf); X_d' and φ are the transient reactance and the power angle. P_m is the mechanical power input through the mechanical shaft.

Regarding $[\Delta V_t \ \Delta \theta_t]^T$, ΔP_m , $\Delta E'$ as input perturbations, (23) can be represented as:

$$\begin{bmatrix} \Delta \dot{\delta} \\ \Delta \dot{\omega} \end{bmatrix} = \begin{bmatrix} 0 & 1 \\ -\frac{V_t E'}{M X_d'} \cos(\varphi) & -\frac{D}{M} \end{bmatrix} \begin{bmatrix} \Delta \delta \\ \Delta \omega \end{bmatrix} + \mathbf{u} \quad (24)$$

where

$$\begin{aligned}
 \mathbf{u} &= \begin{bmatrix} 0 & 0 \\ -\frac{E'}{M X_d'} \sin(\varphi) & \frac{V_t E'}{M X_d'} \cos(\varphi) \end{bmatrix} \begin{bmatrix} \Delta V_t \\ \Delta \theta_t \end{bmatrix} + \begin{bmatrix} 0 \\ \frac{1}{M} \end{bmatrix} [\Delta P_m] \\
 &+ \begin{bmatrix} 0 \\ -\frac{V_t}{M X_d'} \sin(\varphi) \end{bmatrix} [\Delta E']
 \end{aligned} \quad (25)$$

This means that the forced oscillations from both excitation systems (exciters and PSSs) and turbine governors will manifest themselves in rotor dynamics. In either case, $\Delta E'$ or ΔP_m with forced oscillations can be represented as a Fourier series $\sum_{i=1}^l (x_i \sin(\omega_{F_i} t) + y_i \cos(\omega_{F_i} t))$. Assuming the input perturbation from $[\Delta V_t, \Delta \theta_t]^T$ is relatively small, (24) can be represented approximately as:

$$\begin{aligned}
 \begin{bmatrix} \Delta \dot{\delta} \\ \Delta \dot{\omega} \end{bmatrix} &= \begin{bmatrix} 0 & 1 \\ -\frac{V_t E'}{M X_d'} \cos(\varphi) & -\frac{D}{M} \end{bmatrix} \begin{bmatrix} \Delta \delta \\ \Delta \omega \end{bmatrix} \\
 &+ \sum_{i=1}^l \left(\begin{bmatrix} 0 \\ \mathbf{a}_i \end{bmatrix} \sin(\omega_{F_i} t) + \begin{bmatrix} 0 \\ \mathbf{b}_i \end{bmatrix} \cos(\omega_{F_i} t) \right)
 \end{aligned} \quad (26)$$

which is a special form of (1)-(2) for the single machine infinite bus system. It should be noted that (23) may be extended to a multi-generation system following the procedure described in [45] (Chapter 7). As such, it is believed that rotor dynamics are sufficient to describe the power system with sustained forced oscillations, which is also validated in numerical studies presented in Section V-VI.

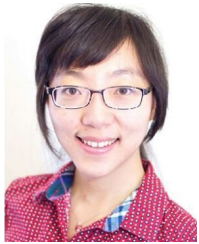
REFERENCES

- [1] D. N. Kosterev, C. W. Taylor, and W. A. Mittelstadt, "Model validation for the August 10, 1996 WSCC system outage," *IEEE transactions on power systems*, vol. 14, no. 3, pp. 967–979, 1999.
- [2] J. Ma, P. Zhang, H. Fu, B. Bo, and Z. Dong, "Application of Phasor Measurement Unit on Locating Disturbance Source for Low-Frequency Oscillation," *IEEE Transactions on Smart Grid*, vol. 1, no. 3, pp. 340–346, 2010.
- [3] N. Rostamkolai, R. Piwko, and A. Matusik, "Evaluation of the impact of a large cyclic load on the LILCO power system using time simulation and frequency domain techniques," *IEEE transactions on power systems*, vol. 9, no. 3, pp. 1411–1416, 1994.

- [4] P. Kundur, N. J. Balu, and M. G. Lauby, *Power system stability and control*. McGraw-hill New York, 1994, vol. 7.
- [5] D. Trudnowski and J. Pierre, "Overview of algorithms for estimating swing modes from measured responses," in *2009 IEEE Power & Energy Society General Meeting*. IEEE, 2009, pp. 1–8.
- [6] L. Vanfretti, L. Doseik, J. W. Pierre, D. Trudnowski, J. H. Chow, R. García-Valle, and U. Aliyu, "Application of ambient analysis techniques for the estimation of electromechanical oscillations from measured PMU data in four different power systems," *European Transactions on Electrical Power*, vol. 21, no. 4, pp. 1640–1656, 2011.
- [7] IEEE PES PSDP Committee and PSSC Subcommittee. IEEE PES Task Force on Oscillation Source Location. [Online]. Available: <http://web.eecs.utk.edu/~kaisun/TF/index.html> (accessed 2020, December 16th)
- [8] U. Agrawal, J. W. Pierre, J. Follum, D. Duan, D. Trudnowski, and M. Donnelly, "Locating the source of forced oscillations using PMU measurements and system model information," in *2017 IEEE Power Energy Society General Meeting*, 2017, pp. 1–5.
- [9] S. Chevalier, P. Vorobev, and K. Turitsyn, "Using Effective Generator Impedance for Forced Oscillation Source Location," in *2019 IEEE Power Energy Society General Meeting (PESGM)*, 2019, pp. 1–1.
- [10] Y. Xu, Z. Gu, and K. Sun, "Location and Mechanism Analysis of Oscillation Source in Power Plant," *IEEE Access*, 2020.
- [11] T. Huang, N. M. Freris, P. R. Kumar, and L. Xie, "A Synchrophasor Data-Driven Method for Forced Oscillation Localization Under Resonance Conditions," *IEEE Transactions on Power Systems*, vol. 35, no. 5, pp. 3927–3939, 2020.
- [12] L. Chen, Y. Min, and W. Hu, "An energy-based method for location of power system oscillation source," *IEEE Transactions on Power Systems*, vol. 28, no. 2, pp. 828–836, 2013.
- [13] S. Maslennikov and E. Litvinov, "ISO New England Experience in Locating the Source of Oscillations Online," *IEEE Transactions on Power Systems*, vol. 36, no. 1, pp. 495–503, 2021.
- [14] S. L. Brunton, J. L. Proctor, and J. N. Kutz, "Discovering governing equations from data by sparse identification of nonlinear dynamical systems," *Proceedings of the national academy of sciences*, vol. 113, no. 15, pp. 3932–3937, 2016.
- [15] L. Zhang and H. Schaeffer, "On the convergence of the SINDY algorithm," *Multiscale Modeling & Simulation*, vol. 17, no. 3, pp. 948–972, 2019.
- [16] S. L. Brunton, J. L. Proctor, and J. N. Kutz, "Sparse identification of nonlinear dynamics with control (SINDYc)," *IFAC-PapersOnLine*, vol. 49, no. 18, pp. 710–715, 2016.
- [17] E. Kaiser, J. N. Kutz, and S. L. Brunton, "Sparse identification of nonlinear dynamics for model predictive control in the low-data limit," *Proceedings of the Royal Society A*, vol. 474, no. 2219, p. 20180335, 2018.
- [18] S. Maslennikov, B. Wang, Q. Zhang, a. Ma, a. Luo, a. Sun, and E. Litvinov, "A test cases library for methods locating the sources of sustained oscillations," in *2016 IEEE Power and Energy Society General Meeting (PESGM)*, 2016, pp. 1–5.
- [19] S. Maslennikov, B. Wang, Q. Zhang, F. Ma, X. Luo, K. Sun, and E. Litvinov. "Test Cases Library of Power System Sustained Oscillations". [Online]. Available: <https://web.eecs.utk.edu/~kaisun/Oscillation> (accessed 2020, December 16th)
- [20] M. A. M. Ariff and B. C. Pal, "Coherency identification in interconnected power system—an independent component analysis approach," *IEEE Transactions on Power Systems*, vol. 28, no. 2, pp. 1747–1755, 2013.
- [21] X. Wang, J. W. Bialek, and K. Turitsyn, "PMU-based estimation of dynamic state Jacobian matrix and dynamic system state matrix in ambient conditions," *IEEE Transactions on Power Systems*, vol. 33, no. 1, pp. 681–690, 2017.
- [22] H. Sheng and X. Wang, "Online measurement-based estimation of dynamic system state matrix in ambient conditions," *IEEE Transactions on Smart Grid*, vol. 11, no. 1, pp. 95–105, 2020.
- [23] T. Odun-Ayo and M. L. Crow, "An analysis of power system transient stability using stochastic energy functions," *International Transactions on Electrical Energy Systems*, vol. 23, no. 2, pp. 151–165, 2013.
- [24] I. Zenelis, X. Wang, and I. Kamwa, "Online PMU-Based Wide-Area Damping Control for Multiple Inter-Area Modes," *IEEE Transactions on Smart Grid*, vol. 11, no. 6, pp. 5451–5461, 2020.
- [25] L. Vanfretti and J. H. Chow, "Analysis of power system oscillations for developing synchrophasor data applications," in *2010 IREP Symposium Bulk Power System Dynamics and Control - VIII (IREP)*, 2010, pp. 1–17.
- [26] G. Zweigle, D. Finney, and R. Moxley, "Adding shaft angle measurement to generator protection and monitoring," in *2013 66th Annual Conference for Protective Relay Engineers*, 2013, pp. 549–556.
- [27] D. J. Trudnowski, "Estimating Electromechanical Mode Shape From Synchrophasor Measurements," *IEEE Transactions on Power Systems*, vol. 23, no. 3, pp. 1188–1195, 2008.
- [28] N. Zhou, S. Lu, R. Singh, and M. A. Elizondo, "Calibration of reduced dynamic models of power systems using phasor measurement unit (PMU) data," in *2011 North American Power Symposium*. IEEE, 2011, pp. 1–7.
- [29] T. Rahman, S. Sankaran, N. Seeley, and K. Garg, "Capturing generator rotor angle and field quantities - SDG amp:E experience and approach to using nontraditional generator measurements," in *2016 69th Annual Conference for Protective Relay Engineers (CPRE)*, 2016, pp. 1–9.
- [30] J. Van Brakel. "Robust peak detection algorithm using Z-scores". [Online]. Available: <https://stackoverflow.com/questions/22583391/peak-signal-detection-in-realtime-timeseries-data> (accessed December 16th)
- [31] H. Ye, Y. Liu, P. Zhang, and Z. Du, "Analysis and Detection of Forced Oscillation in Power System," *IEEE Transactions on Power Systems*, vol. 32, no. 2, pp. 1149–1160, 2017.
- [32] Q. Tang and X. Wang, "A Periodogram-Based Method to Identify Forced and Natural Oscillations Using PMUs," in *2019 IEEE Power & Energy Society General Meeting (PESGM)*. IEEE, 2019, pp. 1–5.
- [33] X. Wang and K. Turitsyn, "Data-driven diagnostics of mechanism and source of sustained oscillations," *IEEE Transactions on Power Systems*, vol. 31, no. 5, pp. 4036–4046, 2015.
- [34] C. Leys, C. Ley, O. Klein, P. Bernard, and L. Licata, "Detecting outliers: Do not use standard deviation around the mean, use absolute deviation around the median," *Journal of Experimental Social Psychology*, vol. 49, no. 4, pp. 764–766, 2013.
- [35] IEEE, "IEEE Standard for Synchrophasor Data Transfer for Power Systems," *IEEE Std C37.118.2-2011 (Revision of IEEE Std C37.118-2005)*, pp. 1–53, 2011.
- [36] G. Lindfield and J. Penny, *Numerical methods: using MATLAB*. Academic Press, 2018.
- [37] B. J. Pierre, F. Wilches-Bernal, D. A. Schoenwald, R. T. Elliott, D. J. Trudnowski, R. H. Byrne, and J. C. Neely, "Design of the pacific DC intertie wide area damping controller," *IEEE Transactions on Power Systems*, vol. 34, no. 5, pp. 3594–3604, 2019.
- [38] B. Hill, D. Trudnowski, and J. Wold, "Frequency estimation for the PDCI inter-area oscillation damping controller," in *2016 IEEE Power and Energy Society General Meeting (PESGM)*, 2016, pp. 1–5.
- [39] C. S. Kulkarni, A. Gupta, and P. F. Lermusiaux, "Sparse Regression and Adaptive Feature Generation for the Discovery of Dynamical Systems," in *International Conference on Dynamic Data Driven Application Systems*. Springer, 2020, pp. 208–216.
- [40] F. Milano, "Power System Analysis Toolbox: Quick Reference Manual for PSAT version 2.1. 2," 2008.
- [41] Powertech Labs Inc. "TSAT TRANSIENT SECURITY ASSESSMENT TOOL". [Online]. Available: <https://powertechlabs.com/tsat/> (accessed 2022, May 11th)
- [42] H. Yuan, R. S. Biswas, J. Tan, and Y. Zhang, "Developing a reduced 240-bus wecc dynamic model for frequency response study of high renewable integration," in *2020 IEEE/PES Transmission and Distribution Conference and Exposition (T&D)*. IEEE, 2020, pp. 1–5.
- [43] IEEE PSE Contest Committee. "2021 IEEE-NASPI Oscillation Source Location Contest". [Online]. Available: <http://web.eecs.utk.edu/~kaisun/Oscillation/2021Contest/>
- [44] S. Maslennikov, B. Wang, and E. Litvinov, "Dissipating energy flow method for locating the source of sustained oscillations," *International Journal of Electrical Power & Energy Systems*, vol. 88, pp. 55–62, 2017.
- [45] P. W. Sauer, M. A. Pai, and J. H. Chow, *Power system dynamics and stability: with synchrophasor measurement and power system toolbox*. John Wiley & Sons, 2017.



Yaojie Cai received the the B.S. and MSc degrees in electrical and computer engineering from the University of Manitoba, Winnipeg, MB, Canada. He was a Research Assistant with Royal Military College of Canada, Kingston, ON, Canada. He is currently working toward the Ph.D. degree in electrical and computer engineering with McGill University, QC, Canada. His research interests include data analytics, power system stability and control.



Xiaozhe Wang (Senior Member, IEEE) is currently an Associate Professor in the Department of Electrical and Computer Engineering at McGill University, Montreal, QC, Canada. She received the Ph.D. degree in the School of Electrical and Computer Engineering from Cornell University, Ithaca, NY, USA, in 2015, and the B.S. degree in Information Science & Electronic Engineering from Zhejiang University, Zhejiang, China, in 2010. Her research interests are in the general areas of power system stability and control, uncertainty quantification in

power system security and stability, and wide-area measurement system (WAMS)-based detection, estimation, and control. She is serving on the editorial boards of *IEEE Transactions on Power Systems*, *Power Engineering Letters*, and *IET Generation, Transmission and Distribution*.



Géza Joós (Life Fellow, IEEE) graduated from McGill University, Montreal, Canada, with an M.Eng. and Ph.D. in Electrical Engineering. He is a Professor in the Department of Electrical and Computer Engineering Department at McGill University (since 2001). He holds a Canada Research Chair in Powering Information Technologies (since 2004). His research interests are in distributed energy resources, including renewable energy resources, advanced distribution systems and microgrids. He was previously with ABB, the Université du Québec and

Concordia University (Montreal, Canada). He is active in IEEE Standards Association working groups on distributed energy resources and microgrids. He is a Fellow of CIGRE, and the Canadian Academy of Engineering.



Innocent Kamwa (Fellow, IEEE) obtained his Ph.D. in Electrical Engineering from Laval University, Quebec, QC, Canada in 1989. A full professor in the Department of Electrical Engineering and Tier 1 Canada Research Chair in Decentralized Sustainable Electricity Grids for Smart Communities at Laval University, he was previously a researcher at Hydro-Québec's Research Institute, specializing in the dynamic performance and control of power systems. He was also the Chief Scientist for Hydro-Québec's Smart Grid Innovation Program and an international

consultant in power grid simulation and network stability. Dr. Kamwa is a past Editor-in-Chief of *IET Generation, Transmission and Distribution*, and is currently the Editor-in-Chief of *IEEE Power and Energy Magazine* and an Associate Editor of *IEEE Transactions on Power Systems*. A Fellow of the Canadian Academy of Engineering and Fellow of the IEEE for his innovations in power system control, he is also the 2019 recipient of the IEEE Charles Proteus Steinmetz and Charles Concordia Awards.